Agriculture, Ecosystems and Environment 269 (2019) 156–166

Contents lists available at ScienceDirect

Agriculture, Ecosystems and Environment

journal homepage: www.elsevier.com/locate/agee

Heuristic cellular automaton model for simulating soil organic carbon under land use and climate change: A case study in eastern China

Xiao-Dong Song[a], Jian-Yi Yang[b], Ming-Song Zhao[c], Gan-Lin Zhang[a,d,*], Feng Liu[a], Hua-Yong Wu[a]

[a] State Key Laboratory of Soil and Sustainable Agriculture, Institute of Soil Science, Chinese Academy of Sciences, Nanjing, 210008, China
[b] Sichuan Quality Supervision and Testing Center of Surveying and Mapping Product, Chengdu, 610041, China
[c] Institute of Survey and Mapping, Anhui University of Science and Technology, Huainan, 232001, China
[d] University of the Chinese Academy of Sciences, Beijing, 100049, China

ARTICLE INFO

Keywords:
Soil carbon sequestration
Spatial prediction
Urbanization
Artificial neural network
Carbon migration

ABSTRACT

The concentration of soil organic carbon (SOC) is one of the most important soil properties, and its spatio-temporal variability greatly affects the global climate and agroecology. To investigate the effects of land use and climate change on SOC, a heuristic cellular automaton (HCA) model was proposed and applied to a plains area in eastern China with a high population density and rapid urbanization rate. The HCA model was designed to simulate the geographical variation in SOC dynamics over the long term (2080), and lateral carbon (C) migration is represented by revised neighbourhood variables at the macro scale. Three widely used soil mapping techniques were applied for comparison: multiple linear regression (MLR), support vector machine (SVM) and kriging with external drift (KED). The HCA model enhanced the accuracy of the predicted SOC by 15.27% over MLR, 12.31% over SVM and 10.98% over KED. Future land use maps were produced using legacy land use data and artificial neural network-based cellular automata (CA), and the simulation results showed the rapid urbanization of this area, where the percentage of cropland declined by 23.75% and that of village/urban areas increased by 22.90% from 2010 to 2080. The overall SOC concentrations are anticipated to increase by 2080 given the rising mean annual air temperature and mean annual precipitation. Our results also suggested that land use change clearly influenced the change in soil C, with village/urban areas exhibiting higher SOC than cropland. To provide stakeholders with accurate soil information, it is important to understand the comprehensive impacts of land use and climate change on soil evolution; this study illustrates the value of integrating pedogenetic information in soil C simulation models.

1. Introduction

Soil organic carbon (SOC) concentrations generally play a pivotal role in soil functioning. The diversiform tillage activities and continual changes in land use and climate promote soil evolution (Leifeld et al., 2005). SOC affects various physical and chemical processes in the soil, and its spatio-temporal pattern is characterized by heterogeneity and uncertainty (Dorji et al., 2014; Ye et al., 2016). Dynamic modelling of SOC change is necessary for the effective monitoring of SOC stocks and for agricultural management.

Understanding soil-forming factors is critical for the simulation of carbon (C) dynamics. The SOC allocation of primary components is altered by both macro- (e.g., climate change and topography) and micro-factors (e.g., microbial decomposition rates) (Jandl et al., 2014). Thus, organic matter is affected by multiple interacting environmental controls, although one factor might be dominant. The most important variables affecting these factors are typically identified based on case studies (Paz et al., 2016). In general, climate, land use and soil type act as the main controls of SOC in different landscapes (López-Ulloa et al., 2005; Li and Shao, 2014; Paz et al., 2016). Anthropogenic activities are accelerating the rate of land use change and play an important role in impacting soil evolution in terms of fertilization, deforestation, urbanization and so on (Gelaw et al., 2014; Xiong et al., 2014; Ross et al., 2016). These environmental variables can be parameterized in predictive models to enhance SOC stock estimation (Dorji et al., 2014; Jandl et al., 2014; Paz et al., 2016).

The spatial pattern of the SOC concentration can be discretely modelled as a regular grid-based map. This method, known as digital soil mapping (DSM), has been widely applied by pedologists, and it differs from mapping models assuming that soil variation is

* Corresponding author at: State Key Laboratory of Soil and Sustainable Agriculture, Institute of Soil Science, Chinese Academy of Sciences, Nanjing, 210008, China.
E-mail address: glzhang@issas.ac.cn (G.-L. Zhang).

https://doi.org/10.1016/j.agee.2018.09.034
Received 20 October 2017; Received in revised form 26 September 2018; Accepted 30 September 2018
Available online 09 October 2018
0167-8809/ © 2018 Elsevier B.V. All rights reserved.

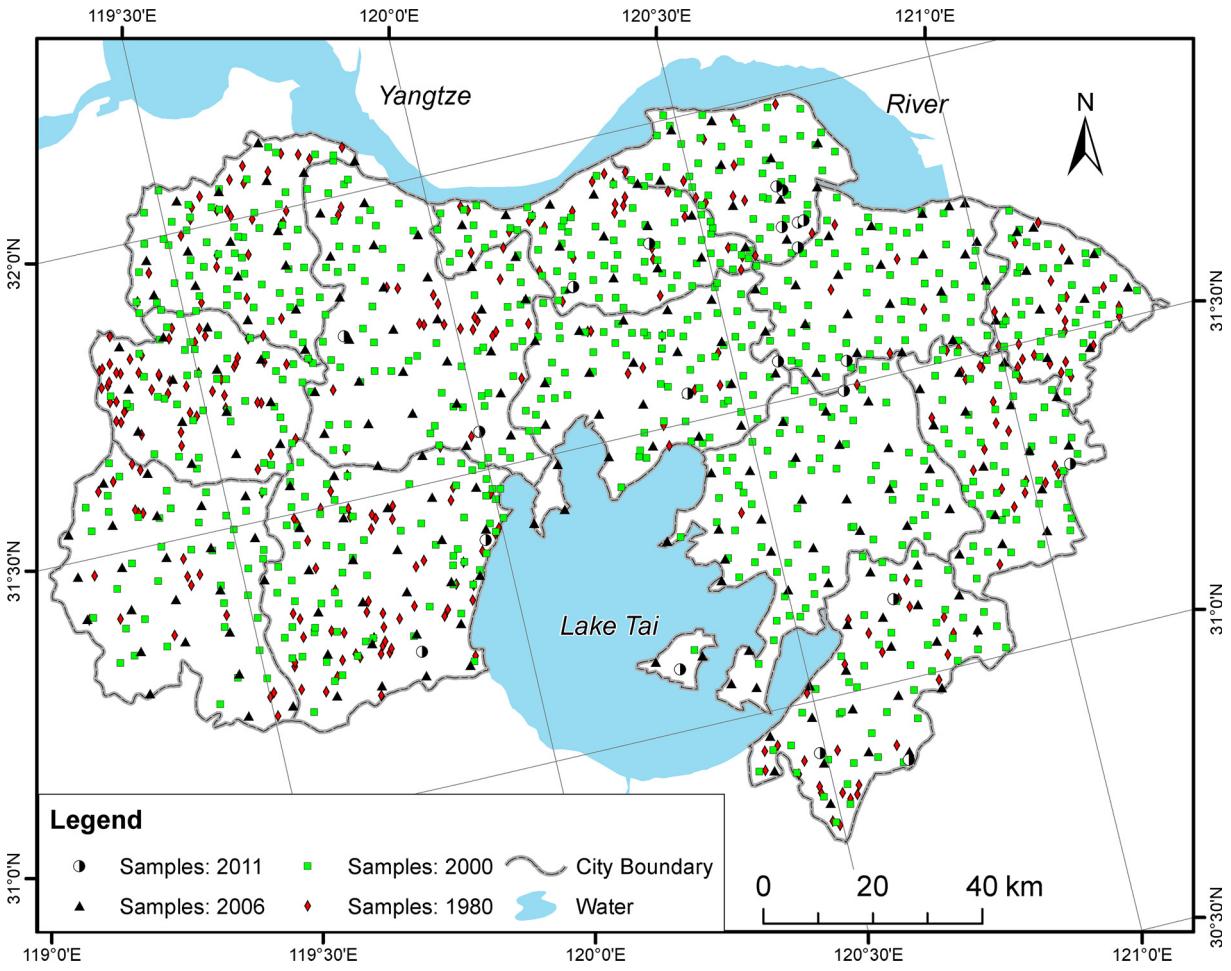

Fig. 1. Location of the study area.

homogeneous within a given landscape unit (Jandl et al., 2014). Numerous studies have attempted to identify the most important predictors (Bodaghabadi et al., 2011), compare predictive models (Grunwald, 2009) and summarize the regional changes in SOC stocks (Dorji et al., 2014). While considerable progress has also been achieved in spatio-temporal simulations (Jandl et al., 2014; Yigini and Panagos, 2016), shortcomings remain, particularly with respect to the spatial heterogeneity of SOC. For instance, due to the fragmented ownership of cropland in China, farms with an area of a few tenths of a hectare engage in variable cultivation practices (Song et al., 2016). Detailed soil information can be obtained only through costly field sampling, which hampers the production of up-to-date soil maps using DSM approaches. Furthermore, how to select the most useful predictors remains a challenge for model calibration, as models might be susceptible to noisy training data. In addition, given the same soil data and environmental predictors, the predictors selected based on stepwise methods (Kempen et al., 2011; Guo et al., 2015) or machine learning (Taghizadeh-Mehrjardi et al., 2016) might differ. This situation does not conform well to pedogenic theory, as some important predictors would be removed due to the low correlations between soil properties of interest and predictors, such as parent material, climate and terrain attributes. Various process-based and data-driven models have improved soil C simulations in the context of land use and climate change (Yu et al., 2013; Jandl et al., 2014; Zhang et al., 2016a; Muñoz-Rojas et al., 2017). However, few studies have quantified the effect of lateral C fluxes on SOC dynamics in terms of the transfer of dissolved organic C (DOC) and particulate organic C (POC) in paddy fields, soil erosion and other land surface processes, although these impacts are far from negligible (Parton et al., 1987; Almagro and Martínez-Mena, 2014; Wang et al., 2017; Wei et al., 2017). It may be plausible to use soil data sampled in different periods; however, in ecosystem modelling using complex functions, the requirement of numerous parameters might prohibit easy implementation, and ill-defined parameters will greatly bias simulation performance (Li et al., 2016a; Brilli et al., 2017).

Cellular automata (CA) models have been of interest in geographic modelling for over fifty years, including land use change simulations (Aburas et al., 2016), geomorphic process simulations (Fonstad, 2013), and seismicity descriptions (Jiménez, 2013), and these models show obvious advantages over empirical models and physically based models. CA models are composed of a regular grid of cells with several states that are affected by local interactions with neighbourhoods and are transformed according to a given rule. Therefore, CA models have been widely adopted to simulate limited states (Oku and Aihara, 2010; Basse et al., 2014). Furthermore, based on the paradigm of CA, macroscopic cellular automata (MCA) have been proposed to model infinite states through a discrete formulation, such as groundwater modelling (Ravazzani et al., 2011), ecohydrological dynamics modelling (Mendicino et al., 2015) or soil moisture modelling (Song et al., 2016). Compared with physically based equations, the transformation rules can be trained via machine learning techniques, and the goodness-of-fit of these models can be evaluated by quality indices (Wang and Li, 2011; Song et al., 2016). Regarding the source of C migration, SOC enrichment will greatly affect the redistribution process, and thus, calculating the neighbourhood state of SOC in terms of CA cells is promising to improve the simulation of soil C migration from the perspective of a "black box" by combining neighbourhood variables with prediction methods.

In this study, a heuristic cellular automaton (HCA) model was

proposed to predict SOC concentrations in eastern China. As a general rule, soil-forming factors were considered, and dominant predictors were incorporated in the HCA model. To develop an optimal transition rule, two neighbourhood shapes were used to locally simulate the transfer of SOC. After model validation by comparison with three widely used DSM approaches, the HCA model was applied to evaluate the impacts of land use and climate change on soil C dynamics until 2080.

2. Materials and methods

2.1. Study area

The study area is located in southeastern Jiangsu Province, China, ranging from 119°8′ to 121°20′ E and 30°45′ to 31°59′ N and covering an area of 15,744 km^2 (Fig. 1). The study area is bounded in the north by the Yangtze River and in the south by Lake Tai. This area is characterized by a northern subtropical monsoon climate; the mean annual precipitation varies from 1038 mm to 1324 mm, and the mean annual temperature ranges from 15.2 °C to 16.1 °C. The topography is slightly variable, with an average elevation of 12 m a.s.l. and an average slope of 2.5%.

Approximately 56.9% and 5.6% of this area was covered by paddy fields and dry land, respectively, and approximately 17.7% and 6.2% was covered by village and forest, respectively. The land cover has changed rapidly due to intensive anthropogenic activities, and the population density was 1443 km^{-2}. The predominant soil groups were Fe-accumuli-Stagnic Anthrosols and Udi-Alluvic Primosols (Cooperative Research Group on Chinese Soil Taxonomy, 2001).

2.2. Soil data

Four collected datasets were sampled in the 1980s, 2000, 2006 and 2011 and are denoted D1, D2, D3 and D4, respectively (Fig. 1). D1: In total, 305 soil profiles were surveyed from the Second State Soil Survey of China (The National Soil Survey Office, 1995) between 1979 and 1982. The analysed soil properties included SOC, pH, soil texture and other variables. As the exact sampling time was difficult to confirm, the time label was set to 1980. D2: In total, 732 topsoil samples (0–20 cm) were collected in 2000, supported by the Ministry of Science and Technology of the People's Republic of China. D3: In total, 249 topsoil samples were surveyed based on regular sampling, where neighbouring points were located at intervals of 8 km. D4: Twenty-one soil profiles were surveyed for soil series classification based on stratified random sampling (de Gruijter et al., 2006), in which composite samples were collected for each soil horizon. The D1 and D2 datasets were used for the calibration, and the D3 and D4 datasets were employed for validation.

The SOC concentration was analysed by using the Walkley-Black wet oxidation method (Nelson and Sommers, 1982). The vertical distribution of SOC was fitted to 0–20 cm by equal-area quadratic splines (Bishop et al., 1999). Broadly speaking, the field data exhibited a normal distribution, and therefore, transformation with the logarithmic function was not performed (Fig. 2). D2 had the highest mean at 17.31 g kg^{-1}, for which 76% of points were collected in a paddy field, resulting in a high SOC concentration (Chuai et al., 2012). The percentages of paddy samples in D1 and D3 were 57% and 60%, respectively. The SOC means of all datasets for cropland and villages were 15.71 g kg^{-1} and 16.01 g kg^{-1}, respectively.

2.3. HCA modelling procedure

The proposed HCA included four steps (Fig. 3):

***Step 1*:** Observed SOC data and static and dynamic predictors were collected. To determine the impact of land use on SOC dynamics, future land use maps (2010–2080) were produced as dynamic predictors for the HCA model.

Step 2*:** The outlier SOC values were identified, and the SOC data were discretized. Predictors were normalized and selected for HCA model training. Neighbourhood variables of SOC concentrations were initialized to indicate the potential C transport, which was updated during each iterative training of the HCA model in ***Step 3.

***Step 3*:** The HCA model was iteratively trained.

***Step 4*:** The performance of the trained HCA model was validated, and future SOC maps were produced.

The detailed description of these steps can be found in the following four sections, respectively.

2.3.1. Preparation of predictors

In addition to soil data (D1, D2, D3 and D4), we collected fourteen predictors of soil-forming factors (Table 1) that are widely used in the DSM literature (Guo et al., 2015; Were et al., 2015; Heung et al., 2016). In this study, the predictors were classified as dynamic predictors or static predictors depending on whether they varied temporally (Fig. 3).

The static predictors included geological data, soil data and terrain attributes (Table 1 and Fig. 3); Shuttle Radar Topography Mission (SRTM) elevation data with a 90-m spatial resolution were adopted to derive the terrain attributes. A slope length factor was employed to indicate topographically driven soil erosion, and solar radiation was derived via the Solar Radiation function in ArcGIS 10.2 (ESRI, 2014).

Climate data, land use data and neighbourhood variables were employed as dynamic predictors (Table 1 and Fig. 3). The climate data included the mean annual precipitation (MAP) and the mean annual air temperature (MAAT) with a 1-km spatial resolution from the database of the National Meteorological Information Centre of the China Meteorological Administration (CMA) and the WorldClim dataset (Hijmans et al., 2005). The CMA climate data were employed to simulate SOC between 2010 and 2040. Two time periods from WorldClim were used: 2050 (average for 2041–2060) and 2070 (average for 2061–2080). Neighbourhood variables were derived from SOC maps to indicate the effect of current C enrichment on future lateral C migration, and they will be introduced in detail in the following section.

The future land use maps (2010 to 2080) were unavailable for this region, so they were produced by the second author using GeoSOS (http://www.geosimulation.cn). Artificial neural network (ANN)-based CAs, which have been proven to be efficient tools for land use simulation (Li and Yeh, 2002), were employed (Fig. 3). In addition to the terrain attributes (slope and elevation), traffic maps were utilized in the land use simulations to generate Euclidean distance maps, in which each cell represented the distance from highways, roads, and railways as well as the distance to the urban centre. The legacy land use maps from 1980 and 2000 were used for model training to simulate land use changes, and the land use map from 2005 was adopted for model validation (Fig. 3). Six land use types were classified: forest, grassland, cropland, village, wetland and barren. The land use simulation was evaluated according to the confusion matrix, overall accuracy (p_o) and kappa coefficient (Ka) as follows:

$$p_o = \frac{1}{n}\sum_{i=1}^{m} v_i' \tag{1}$$

$$Ka = \frac{p_o - p_e}{1 - p_e} \tag{2}$$

where n and m are the number of items and categories, respectively; v_i' is the number of correctly predicted items for category i and p_e is calculated by:

$$p_e = \frac{1}{n^2}\sum_{i=1}^{m} x_i \hat{x}_i \tag{3}$$

where x_i and $\hat{x}_i$ are the observed and predicted number of items in category i, respectively.

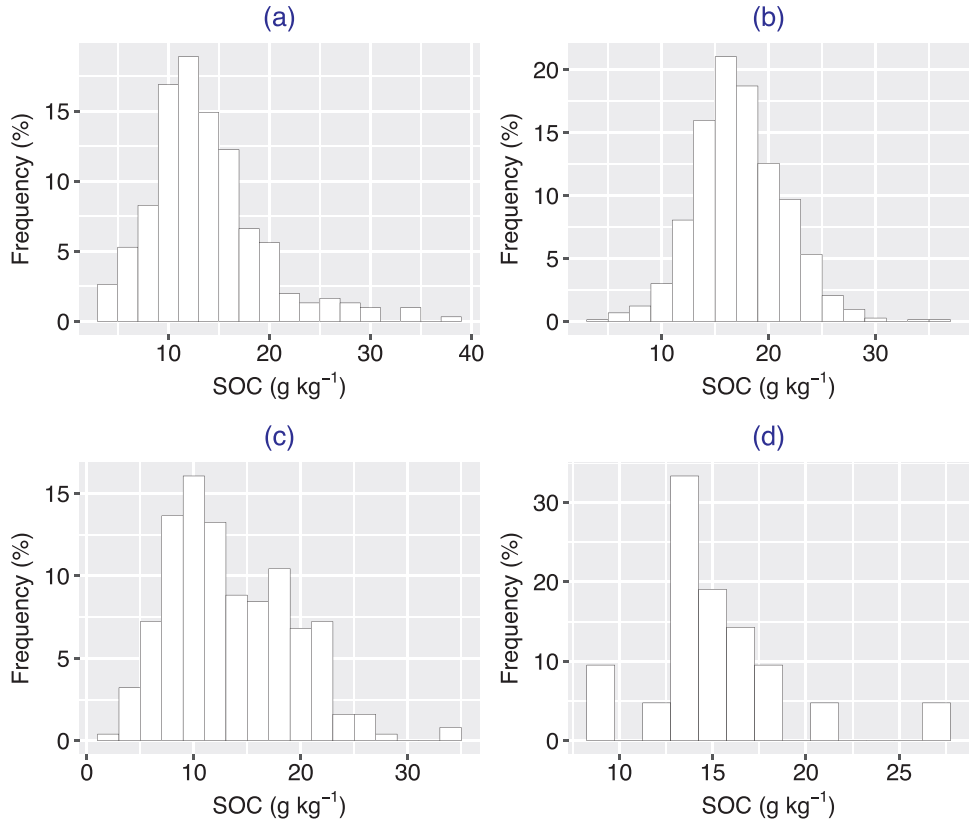

Fig. 2. Histogram of the soil data surveyed in the 1980s (a), 2000 (b), 2006 (c) and 2011 (d).

2.3.2. Pre-processing of input data

Outlier SOC data were identified (Fig. 3). If the SOC value was not within the range of the threshold ($SOC_{mean} \pm 2SOC_{std}$), the outlier was set to the threshold value; SOC_{mean} and SOC_{std} denote the mean and standard deviation of all observations, respectively. Then, all the SOC values were discretized by a transformation function as follows:

$$soc_{int} = \begin{cases} soc - soc \bmod \Delta soc & if\ soc \bmod \Delta soc \le 0.5\Delta soc \\ soc - soc \bmod \Delta soc + \Delta soc & if\ soc \bmod \Delta soc > 0.5\Delta soc \end{cases} \quad (4)$$

where soc_{int} is the discrete SOC value; soc is the observed SOC value; mod is the remainder function; and Δsoc is the threshold value of the discretization. The lower the Δsoc value, the greater the number of SOC states.

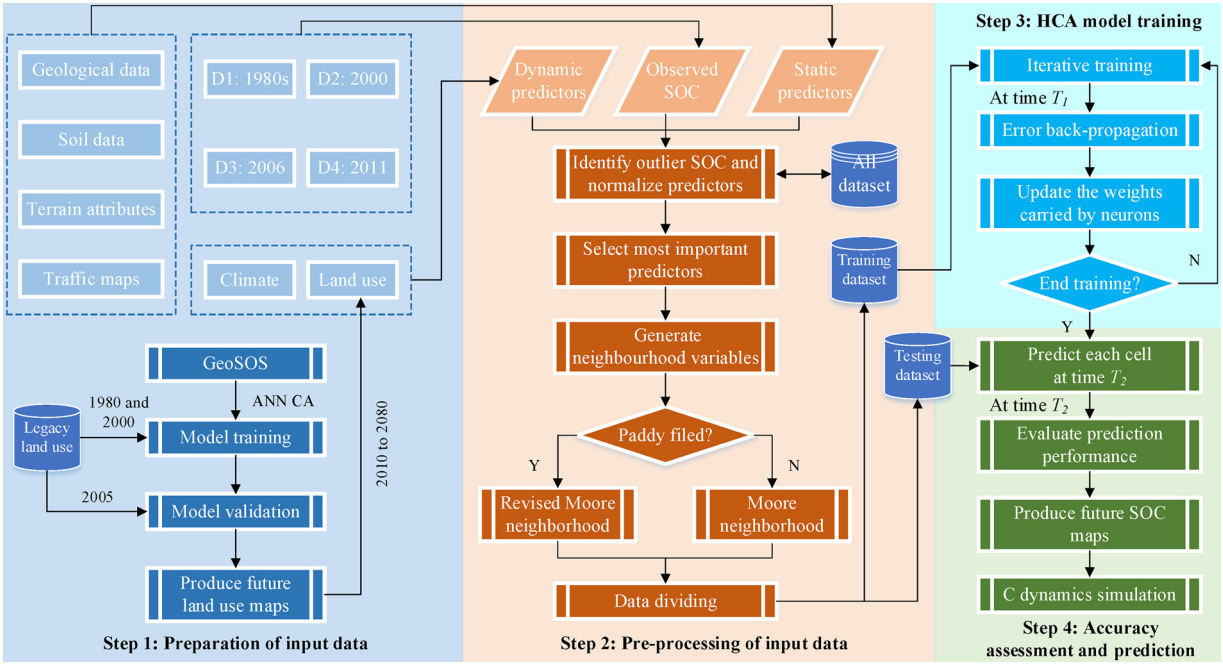

Fig. 3. Workflow of the HCA model. T_1 and T_2 refer to different times.

Table 1
Predictors utilized to predict the spatio-temporal variation of SOC concentrations.

Name	Scale/ resolution	Type [a]	Soil forming[b]	Name	Scale/ resolution	Type	Soil forming
Geological data				*Terrain attributes*			
Geology map	1:250 K	C	P	SRTM DEM	90 m	Q	R
Land use/landscape				Slope	90 m	Q	R
Land cover (digitalized maps in 1980, 2000, 2005 and simulated maps from 2010 to 2080 with intervals of ten years)	1:250 K	C	O	Vertical distance to channel network	90 m	Q	R
Soil data				Slope length	90 m	Q	R
Soil type	1:1 M	C	S	Plan curvature	90 m	Q	R
Neighbourhood variables	90 m	Q	S	Profile curvature	90 m	Q	R
Climate				Relative slope position	90 m	Q	R
Mean annual air temperature (MAAT) (CMA and WorldClim dataset)	1 km	Q	L	Topographic wetness index	90 m	Q	R
Mean annual precipitation (MAP) (CMA and WorldClim dataset)	1 km	Q	L	Solar radiation	90 m	Q	R

[a] C: categorical; Q: quantitative.
[b] R: relief; P: parent material; O: organisms; S: soil properties; L: climate.

Vector layers of predictors were converted to raster format, and all predictors were then resampled to a 90-m spatial resolution. Predictors were normalized to eliminate the effect of magnitude. The most important predictors for the SOC simulation were selected by stepwise regression in both directions (Fig. 3).

Compared with general soil mapping techniques, the CA model highlights lateral SOC migration in terms of neighbourhood variables. It was hypothesized that current C enrichment would greatly impact the lateral SOC migration driven by mass and energy transport, such as the transfer of DOC and POC in paddy fields, soil erosion, tillage and urbanization. Neighbourhood variables of SOC concentrations, that is, the state of the neighbouring cells, were used to indicate the potential C transport, by which C from the central cell might be transferred towards neighbouring (adjacent) cells or vice versa (Fig. 4).

As there were vast areas of paddy fields in the study area, two neighbourhood shapes were used to simulate the local migration of SOC. A revised Moore neighbourhood and a Moore neighbourhood were used for paddy fields and other areas, respectively (Fig. 4). Assuming that the spatial resolution of a cell is w, the revised Moore neighbourhood will cover an area of $21\,w^2$, where the radius r is approximately $2\,w$, and the Moore neighbourhood will cover an area of $9\,w^2$, where the radius, r, is approximately w. Then, focal statistics were performed on the SOC map to produce neighbourhood variables, in which the minimum, maximum, mean and standard deviation were calculated for each grid cell within the surrounding specified neighbourhood (Fig. 4). Four new rasters were generated and utilized as neighbourhood variables. At the initialization stage of the model training (***Step 2***), it was not feasible to calculate neighbourhood variables due to the lack of SOC maps, so a new SOC map was interpolated based on the observed SOC data using ordinary kriging. During HCA model training (***Step 3***), neighbourhood variables were recalculated using a new SOC map that was produced by the trained HCA model in a previous iteration. Finally, all the soil data and predictors were divided into a training dataset, which included soil data and predictors in the 1980s and 2000 (time of *T1*), and a testing dataset, which included the rest of the soil data and predictors (time of *T2*) (Fig. 3).

2.3.3. Model training

As some of the most frequently applied types of artificial intelligence, ANNs are inspired by biological neurons and can fit nonlinear processes, and due to their powerful ability to quantify complex patterns and behaviour, these networks have often been trained to simulate the transition rules of dependent variables for CA (Wang and Li, 2011; Aburas et al., 2016). In this paper, a multi-layer perceptron (MLP) network with a back-propagation algorithm was utilized to derive the SOC transition rules at time *T1* (Fig. 3).

There are three layers of neurons in the MLP network: input, hidden and output. Predictors and SOC data act as the input and output layers, respectively, and neurons in the hidden layer carry weights to represent the linkages between the SOC and predictors. An ANN model is iteratively trained to derive the transition rules of SOC states (Fig. 3). After each iteration, network errors are calculated by error back-propagation in the BP algorithm, and the weights carried by the neurons in the hidden layer are updated. Model training ends when the difference between the weighted summed squared error (SSE) values of two consecutive iterations is less than 0.0001 or the number of iterations reaches 3000 (Fig. 3). The optimal number of neurons in the hidden layer is confirmed by comparing prediction performance of ANN models with different numbers of neurons. For a given number of neurons, the ANN model will run 100 times, and the mean value of the

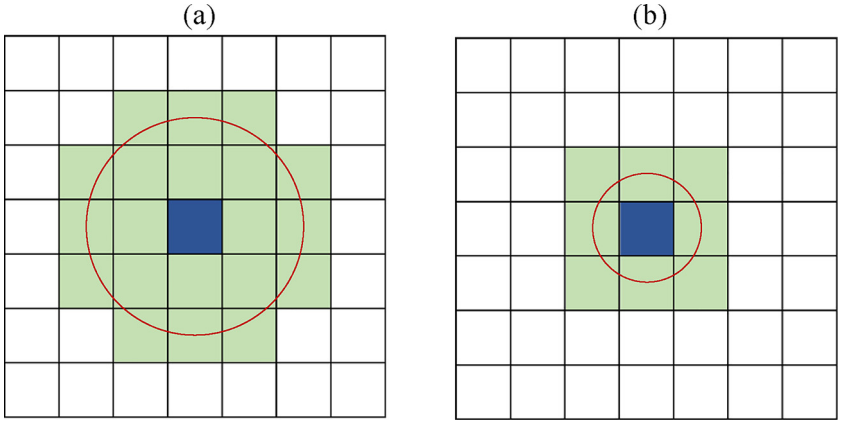

Fig. 4. The revised Moore neighbourhood for paddy fields (a) and the Moore neighbourhood for other areas (b).

validation index is used.

2.3.4. Accuracy assessment and prediction

The SOC value of each cell was predicted based on the calculated transition probability at time *T2*, and the prediction performance was evaluated by statistically measuring prediction errors to verify the capacity for generalization. Finally, the C dynamics could be simulated when the future SOC maps were produced based on the trained HCA model (Fig. 3).

In addition, three widely used predictive techniques were applied for comparison: multiple linear regression (MLR), support vector machine (SVM) and kriging with external drift (KED). MLR is one of the most popular soil mapping techniques and can fit the soil property and environmental variables as a linear combination. SVM can establish an optimal separating hyperplane, enabling regression analysis to be performed with respect to high-dimensional feature spaces; this technique has recently been successfully applied in DSM (Heung et al., 2016). As one of the best linear unbiased predictors, KED integrates environmental variables into the geostatistical interpolation process. After deriving the local means of environmental variables, model residuals are assumed to be spatially dependent and are interpolated by simple kriging. KED shares advantages with geographically weighted regression models that can account for nonstationary correlations and ensure prediction accuracy (Harris et al., 2011).

The performance of the different models was evaluated based on the mean error (ME), mean absolute error (MAE), root-mean-squared error (RMSE) and relative improvement (RI). The RI value was used to indicate the improvement in performance between two prediction techniques as follows:

$$RI = \frac{RMSE_b - RMSE_a}{RMSE_b} 100 \quad (5)$$

where $RMSE_b$ and $RMSE_a$ are the RMSEs of predictive techniques *b* and *a*, respectively.

Map visualization and data analysis were performed in ArcGIS 10.2 and R (version 3.3.1, https://cran.r-project.org/), respectively. The proposed HCA model was implemented in MATLAB (version 2016a, https://www.mathworks.com/), and the MLR, SVM and KED techniques were performed with the R packages “stats” (Wilkinson and Rogers, 1973), “e1071” (Meyer et al., 2017) and “gstat” (Pebesma, 2004), respectively.

3. Results

3.1. Land use simulation

Table 2 shows the confusion matrix between the observed land uses and simulated results in 2005. The comparison of observed and predicted land use is also illustrated in Fig. 5. The overall accuracy and the kappa coefficient for the simulation were 88.20% and 0.78, respectively. Approximately 91.18% of the cropland and 80.70% of the village areas could be accurately predicted, with 62.82% and 19.80% of the total area being covered by cropland and villages, respectively. During 2000–2005, the most frequent land use change was from cropland to village (8.82%), suggesting rapid urbanization (Fig. 5). Even when policy adjustments were not incorporated, the established model was sufficiently robust and could provide additional information about the spatial drivers of land use change. Thus, regarding the conversion probability of land use changes, future projections could be generated with an interval of 10 years.

3.2. HCA model training

After outlier detection and correction of the observations, the threshold value of discretization (Δsoc) was set to 0.5. The optimal parameters of the ANN models were achieved by iterative training. Fig. 6 shows the change rate of weighted SSE with the increase in iteration numbers. At the beginning stage, the error in terms of weighted SSE converged rapidly and then gradually approached stability after 314 iterations. To enhance the learning quality, the number of neurons in the hidden layer was evaluated in terms of RMSE (Fig. 7). Given different numbers of neurons in the hidden layer between 1 and 30, the prediction performance could be obtained, and the optimal number could be confirmed. The architecture with the lowest RMSE was employed in the HCA model.

3.3. Model performance

Table 3 shows the validation indices of SOC predicted by four methods. The highest ME and RMSE were generated by MLR, followed by SVM. The difference between RMSE and MAE was lowest (0.96 g kg^{-1}) for HCA, suggesting low estimation errors. HCA enhanced the accuracy of SOC prediction by 15.27% over MLR, 12.31% over SVM and 10.98% over KED. The evaluation results suggested that the HCA model was sufficiently robust to predict SOC.

Using simulated land use data, digital soil maps for 2006 and 2011 were produced with the four methods (Fig. 8). Overall, none of the maps present a physiographic distribution due to the flat terrain. SOC values generally decreased from southeast to northwest and changed rapidly. High SOC concentrations were generally found in eastern regions, which were primarily covered by wetlands. However, the soil maps produced by the same method showed similar spatial patterns in the two years due to a slight change in the dynamic predictors. A two-sample *t*-test at the 99% confidence level confirmed the significant difference in the simulated maps obtained via the same method. Spatial analysis of map algebra indicated that 38.4% (Fig. 8a), 55.3% (Fig. 8b), 45.4% (Fig. 8c) or 30.3% (Fig. 8d) of the area exhibited an increasing SOC tendency.

3.4. Simulation of future SOC

The future projection of SOC was obtained by updating the dynamic predictors (i.e., land use and climate data) in the established HCA model (Figs. 9 and 10). As seen from Fig. 9, a long-term urbanization process in this area could be anticipated, where the percentage of cropland declined to 39.06% and that of village/urban areas gradually

Table 2
Confusion matrix between the observed land use and simulated results in 2005 (in the number of cells).

	Simulated land uses in 2005							Accuracy (%)
	Land use	Forest	Grassland	Cropland	Village	Wetland	Barren	
Observed land uses in 2005	Forest	104,790	113	8,869	2,323	720	141	89.60
	Grassland	133	1,780	190	80	177	4	75.30
	Cropland	8,590	268	1,076,667	66,451	28,751	41	91.18
	Village	2,042	83	66,080	300,362	3,583	32	80.70
	Wetland	699	144	28,811	3,350	173,530	7	84.02
	Barren	129	5	34	33	16	637	74.59

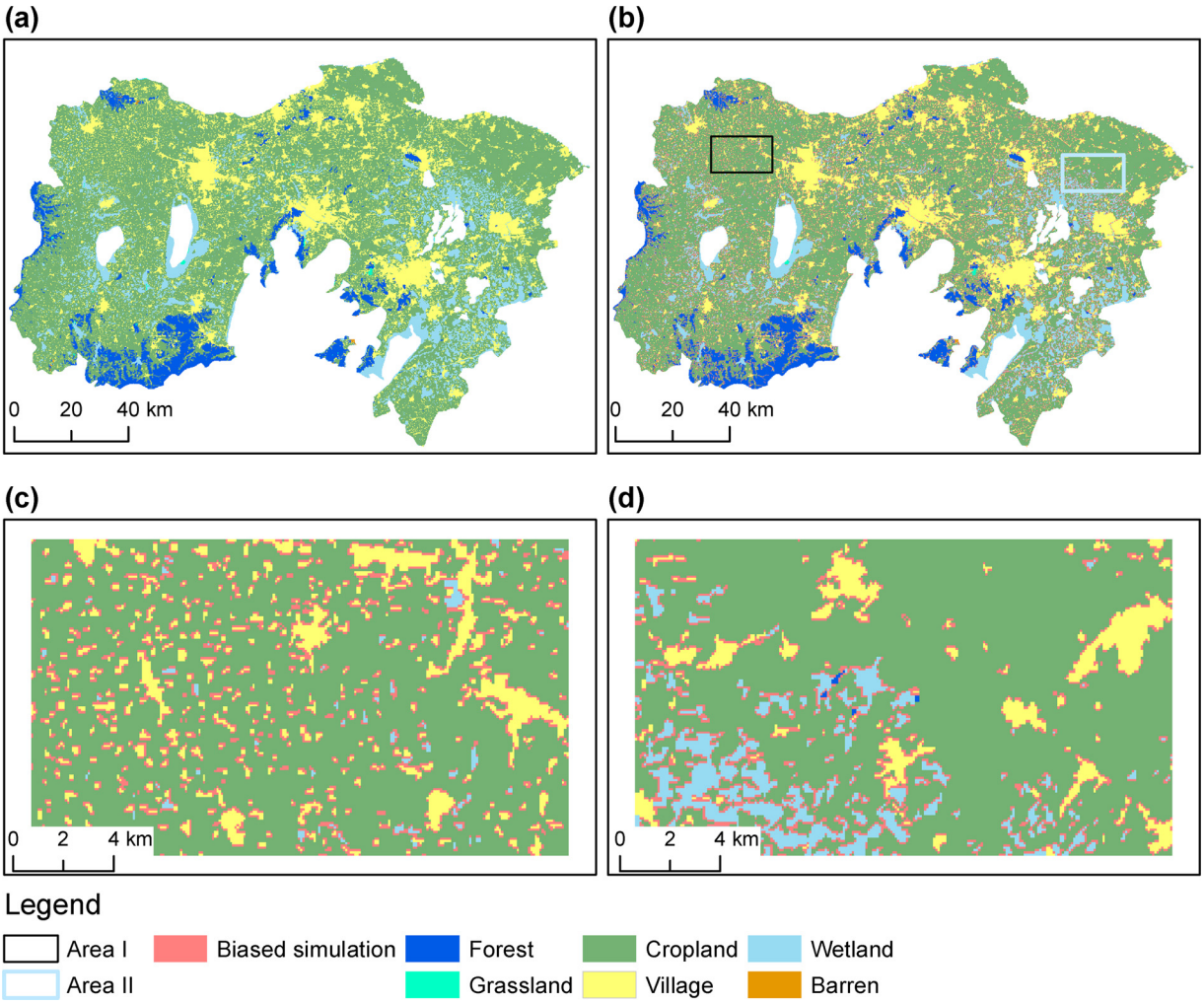

Fig. 5. Comparison between the observed land use (a) and simulated results (b) in 2005 and examples of Area I (c) and Area II (d) with magnification of the simulated results (b).

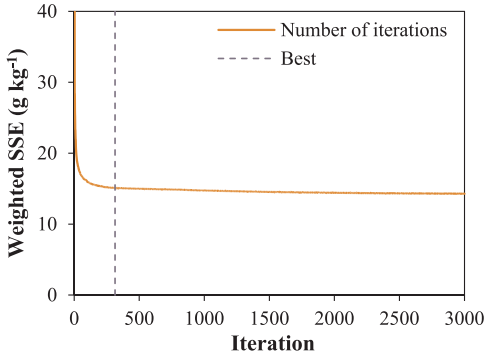

Fig. 6. Distribution of the weighted summed squared error with the increase in iterations. The vertical dashed line indicates the best number of iterations.

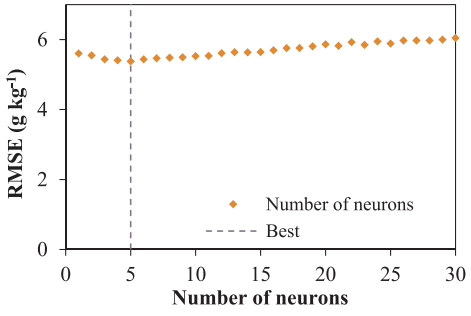

Fig. 7. The RMSE distribution with the increase in neuron numbers. Note that RMSE is the mean value of 100 model runs.

increased to 42.72% in 2080. This simulation concurred with the current high population density (approximately 1443 km^{-2}) and rapid industrialization (the province has the second-highest gross domestic product in China). The mean MAAT and mean MAP increased from 15.5 °C to 17.25 °C and from 1083 mm to 1155 mm, respectively.

The similar spatial pattern of SOC across the years suggested that C dynamics would not be drastically changed according to current observations. Based on the two-sample *t*-test analysis, significant differences were found for each pair of maps with 10 year intervals (Fig. 10). High SOC values were generally generated in the southeastern region. The mean SOC increased from 14.45 g kg^{-1} (2020) to 15.33 g kg^{-1} (2080), suggesting a moderate increasing tendency. Village mean SOC values were slightly higher than those in cropland, which concurred with the observed values (16.01 g kg^{-1} in villages versus 15.71 g kg^{-1} in cropland).

4. Discussion

4.1. Lateral C migration and the HCA model

It is well known that soil properties exhibit high spatial

Table 3
Validation indices of SOC predicted by different methods. Note that soil data for 2006 and 2011 were validated together due to the limited soil data from 2011.

	ME (g kg^{-1})[b]	MAE (g kg^{-1})	RMSE (g kg^{-1})	RI (%)
HCA[a]	0.76	4.31	5.27	–
MLR	2.80	4.97	6.22	15.27
SVM	2.74	4.74	6.01	12.31
KED	2.33	4.58	5.92	10.98

[a] HCA: heuristic cellular automata; MLR: multiple linear regression; SVM: support vector machine; KED: kriging with external drift.
[b] ME: mean error; MAE: mean absolute error; RMSE: root-mean-squared error; RI: relative improvement.

heterogeneity at different scales that are synergistically modified by anthropogenic impacts and internal factors (Grunwald, 2009; Xiong et al., 2014). Thus, in our digital soil model, we preferred to simulate soil variation from the perspective of a "black box" and utilized limited environmental variables as covariates, as the number of soil-forming factors that should be considered is too great and few of them were available.

Although numerous successful case studies and improved techniques have been reported, the effect of neighbouring states of SOC concentrations on C migration has rarely been considered in DSM modelling. Broadly, the dynamics of the terrestrial C cycle are comprehensively affected by physical mobilization (soil redistribution) and chemical transformation (decomposition and sequestration). Various ecological environments result in different C migration and sequestration rates (Ouyang et al., 2014). Soil C fractions might contribute greatly to changes in SOC (Parton et al., 1987), as DOC and POC migrate with soil moisture or surface runoff, along with changes in soil temperature and moisture. The maximal DOC concentrations found in China have been observed in this study area (Gao et al., 2017). Moreover, microaggregate SOC is directly transferred with runoff, and thus, soil erosion is far from being neglectable in this area due to the heavy precipitation during monsoons (Shen and Yan, 2017), even though this area is relatively flat (average slope of 2.5%). The frequency and intensity of rainfall events would greatly affect the size distribution of aggregate in the sediments (Wang et al., 2017), and thus indirectly control SOC concentrations, as high concentrations are usually associated with coarsely sized aggregate fractions (Wei et al., 2017). Unfortunately, due to the complexity of the soil erosion process and hybrid lateral/vertical C fluxes, the impact of soil erosion on C migration

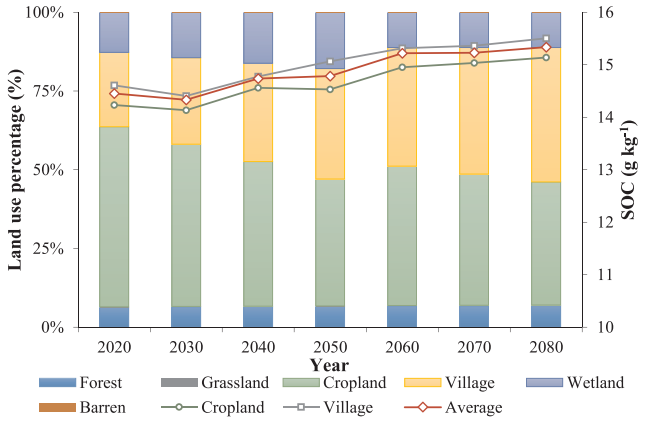

Fig. 9. Simulated land use percentage (%) and mean SOC concentration (g kg^{-1}) in the study area for.2020–2080.

remains unclear and is difficult to parameterize (Almagro and Martínez-Mena, 2014; Wang et al., 2017). In addition to active C pools and soil erosion, detailed information on several soil-forming factors (e.g., tillage, facility agriculture and urbanization) that greatly influence lateral C migration is difficult to collect and to incorporate in the predictive model.

To the best of our knowledge, no corresponding conclusion for quantifying lateral C migration has been reached due to the complexity of soil evolution. Therefore, neighbourhood variables were designed in the HCA model according to a priori knowledge of soil evolution under the assumption that C migration would be directly influenced by adjacent C enrichment. In contrast to analogous soil mapping, we considered the effect of the land use type on C migration and heuristically selected two shapes to generate the neighbourhood variables (Fig. 4). The validation results indicated that the proposed HCA model could effectively enhance prediction performance at the regional scale (Table 3) and might be applicable for areas with extensive paddy fields and heavy precipitation.

The slightly different variations in soil datasets raised concerns regarding best predictor selection (Fig. 2). In the spatio-temporal SOC simulation, the non-linearity of the soil-landscape paradigm was unknown, and it seemed plausible to choose different predictor subsets for different periods. However, this practice is inconsistent with soil evolution theory, in which a few controls (e.g., topography and land use) may be dominant in long-term soil C simulation (Jiang et al., 2014;

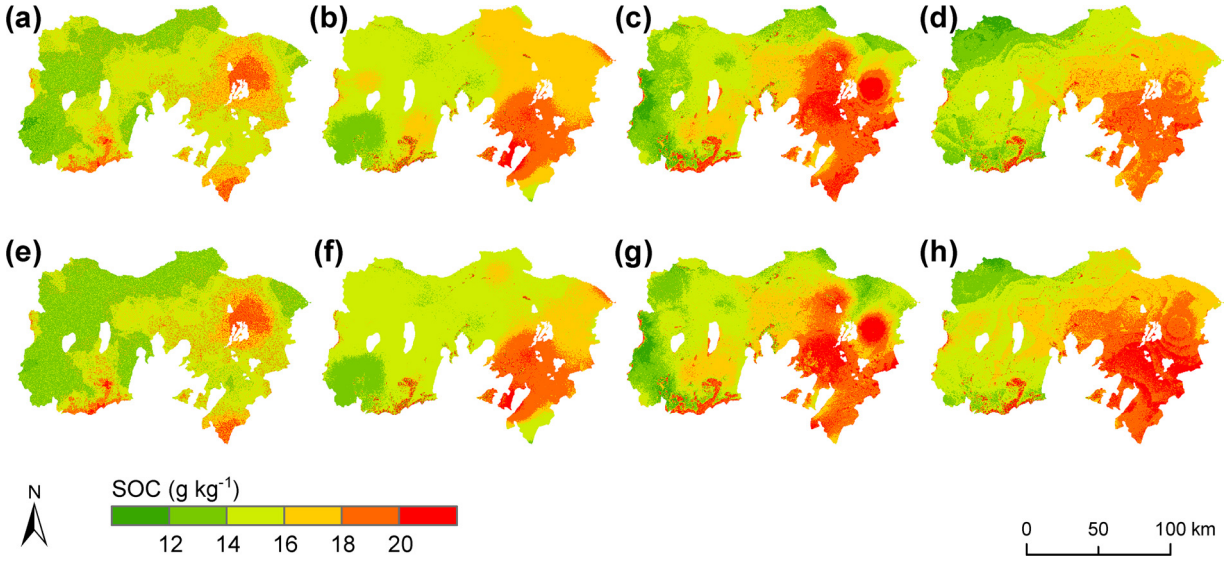

Fig. 8. Spatial prediction of SOC (g kg^{-1}) in 2006 (a, b, c, d) and 2011 (e, f, g, h) estimated by HCA (a, e), MLR (b, f), SVM (c, g) and KED (d, h).

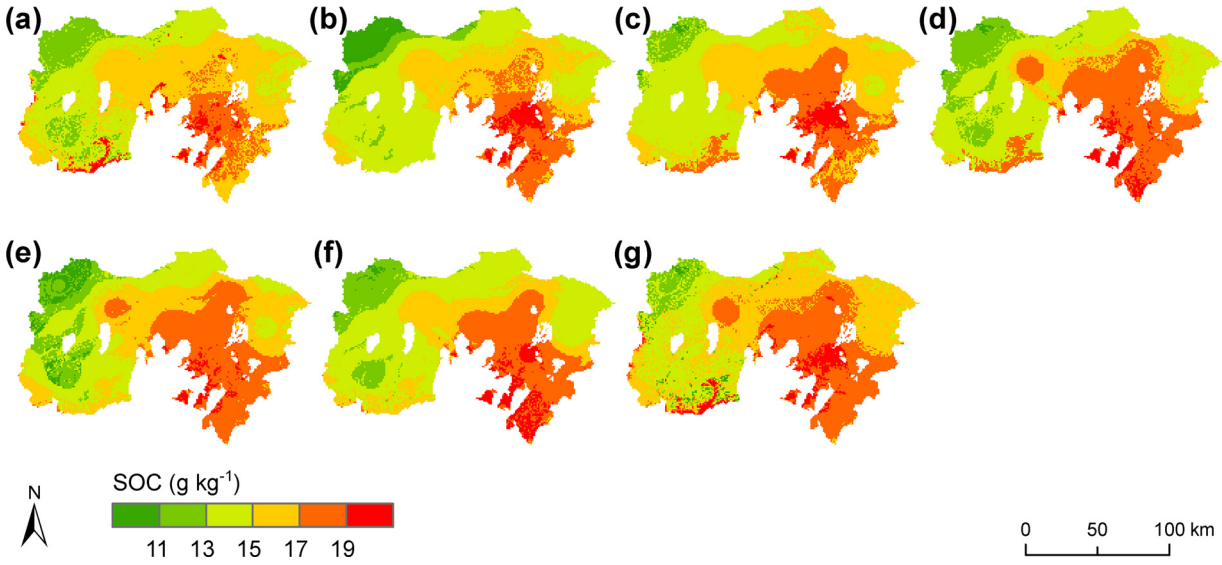

Fig. 10. Distribution of SOC concentrations (g kg^{-1}) in 2020 (a), 2030 (b), 2040 (c), 2050 (d), 2060 (e), 2070 (f) and 2080 (g).

Muñoz-Rojas et al., 2017). Thus, we adopted an invariable predictor set that was conducive to establishing a robust model. Compared with other static predictors, three dynamic predictors (i.e., land use, MAAT and MAP) played moderate roles in the spatio-temporal models (Barthold et al., 2013; Were et al., 2015). Therefore, the same predictor set and the similar spatial pattern of the climatic variables (supplementary material) might have indirectly resulted in similar predictive maps (Figs. 8 and 10), even if the maps were significantly different.

SOC transition rules were derived with the ANN models developed in this study. Thus, the proposed HCA model might share similar features with other DSM models. For example, the HCA model was robust to the noisy predictors and could effectively account for the complicated non-linear relationships between soil properties of interest and environmental variables. Nevertheless, the back-propagation algorithm might be sensitive to the local minimum solution and could be time consuming for training (Li and Yeh, 2002; Wang and Li, 2011).

The uncertainty involved in the predictive procedure should also be identified and assessed. First, climate predictors had a larger spatial resolution than terrain attributes. As the collected predictors had various resolutions, the best option was to adopt the finest resolution in this study (90 m). However, the heterogeneity of SOC within small farmland areas might not be well accounted for, as soil properties in each cell were assumed to be homogeneous by the raster-based techniques. Unfortunately, predictors with a fine resolution (e.g., 10 m) are not available at this time. Therefore, we propose that this task be undertaken in a smaller study area for which detailed ancillary covariates are available. Second, the meteorological and land use data were characterized by various errors (Hijmans et al., 2005). We utilized the uncertainty assessment based on jackknifing (Ließ et al., 2012) to investigate the similarity of SOC maps across different prediction models, for which each was separately executed 100 times and 70% of soil samples (D1 and D2) were randomly selected for modelling during each run. Based on these 100 maps, the standard deviation of each grid cell was computed, and the spatial pattern was adopted to illustrate the uncertainty (Supplementary material). The greater the standard deviation, the higher the prediction uncertainty. In general, the spatial pattern and mean values of these maps suggested that the prediction results across the four considered models were characterized by various degrees of uncertainty. In this study, we utilized soil data sampled in the 1980s and 2000 for calibration and the soil data sampled in 2006 and 2011 for validation. Therefore, the collection of additional soil data to independently validate the produced soil maps is recommended for future research (Brus et al., 2011). Regarding the complexity of SOC dynamics, our proposal provides a viable alternative and must be investigated further through synthetic comparisons.

4.2. SOC under land use change

The simulation results suggested that human disturbance in terms of various types of land use change was crucial for soil C dynamics. An interesting finding was that growing cities acted as C pools and were characterized by the highest SOC based on both observation (Sect. 2.2) and prediction (Fig. 9). This conclusion differed from related studies indicating C stock loss (Hutyra et al., 2011; Zhang et al., 2014; Sallustio et al., 2015). Raciti et al. (2012) reported that the C content was 66% lower in the impervious surface soil than in open areas. In contrast, when we integrally evaluated village/urban SOC, these areas showed higher spatial variability and greater SOC than arable land (Chuai et al., 2012; Vasenev et al., 2012). SOC will quickly decline due to the reduction of vegetation residues when croplands are converted. However, the lost soil C can be gradually restored by incorporating green manure (Garcia-Franco et al., 2015) and long-term fertilization (He et al., 2018). It has been noted that improvement in C sequestration is observed in urban parks (Bae and Ryu, 2015), vegetated land in urban-rural ecotones (Ye et al., 2016) and developed urban areas (Li et al., 2016b). Mineral topsoils obviously contribute to C sequestration in village/urban areas (Dorendorf et al., 2015). In addition, urban management (e.g., urban equilibrium) provides various concepts related to the management of C emissions and sustainable planning in the long term (Stocchero et al., 2017). With the rapid progression of urbanization, cultivated land in ecotones can directly produce vegetables and fruit for townsfolk. Since available cultivated lands are very limited, fertilizer with abundant organic manure is usually applied, to pursue high economic benefits (Ye et al., 2016). Consequently, across all spatial and temporal scales, the dynamic process of soil C will ultimately reach an equilibrium or quasi-equilibrium, in which the soil C lost by soil erosion and human disturbance (e.g., expansion of cultivation) will be compensated by the input from net primary production and tillage fertilization. This situation is illustrated by the SOC change tendency observed in our study (Fig. 9).

Another underappreciated problem is that the SOC concentration increases with the rapid growth of urbanization. In this study, the mean SOC in village and cropland areas changed from 14.61 g kg^{-1} (2020) to 15.52 g kg^{-1} (2080) and from 14.23 g kg^{-1} to 15.14 g kg^{-1}, respectively. Approximately 23.6% of this area was converted from cropland to villages. These findings indicated an obvious C sink in both cropland

and villages. SOC in the converted areas was slighter lower than that in the unchanged village/urban areas, in accordance with recent investigations (Yong et al., 2013; Yoon et al., 2016). Low SOC concentrations were observed in urbanized lands due to the short history of green spaces and low organic matter supply in these areas (Yoon et al., 2016), and some studies have indicated that C storage is concentrated in less urbanized areas (Dorendorf et al., 2015; Sallustio et al., 2015). Inconsistent conclusions can be ascribed to the type of land use change involved. Semi-natural land might be mainly affected by urban growth, where grasslands and wooded lands usually contribute to a high soil organic matter content (Sallustio et al., 2015). In the present study, cropland and wasteland mainly changed to village/urban areas due to the high population density and rapid industrialization. Assuming an absence of C storage beneath impervious surfaces, the definition of an urban boundary raises concerns for SOC estimation, as city fringes might store high C stocks (Dorendorf et al., 2015). This finding is consistent with our results showing that suburban areas contained a large amount of soil C.

4.3. SOC under climate change

To better represent the turnover of SOC, lateral C migration in terms of neighbourhood variables was effectively incorporated into the HCA model, and land use and climate change were considered, as were process-based models such as the Agro-C model (Yu et al., 2013), CarboSOIL model (Muñoz-Rojas et al., 2017), DNDC model (Zhang et al., 2016a) and SPACSYS model (Zhang et al., 2016b). The conclusions of this study were comparable to those from other publications in this area. The macro-distribution of SOC maps was similar to that reported by Chuai et al. (2012), who generally found high SOC concentrations in villages and paddy land. In this area, SOC has increased within the past three decades due to incremental fertilizer application (Zhao et al., 2015) and is expected to steadily increase under all climate scenarios in the long term (Yu et al., 2013; Zhang et al., 2016a).

As described above, climate change did not affect the SOC concentration on a relatively short time scale, but it might dominate the SOC dynamics in the long term. According to the uncertainty evaluation, the WorldClim dataset captures climate variation more accurately in flat areas than in the mountains (Hijmans et al., 2005). Our results suggested that the SOC concentration has gradually increased with increasing air temperature and precipitation, which was consistent with related studies (Jiang et al., 2014; Yigini and Panagos, 2016; Zhang et al., 2016b). This finding can be ascribed to the high conversion efficiency of input C promoted by increasing precipitation (Yu et al., 2012). Assuming that the air temperature is an augmenting factor, the decomposition of soil organic matter would speed up due to the thermodynamic mechanism. In contrast, Zhang et al. (2016a) reported that cropland in this area acted as a C sink under warming conditions. It is worth noting that our conclusions might not be applicable to arid areas. Muñoz-Rojas et al. (2017) investigated the CarboSOIL model by integrating global climate data from northern Egypt, where the latitude is approximately the same as that of the current study area but the annual rainfall is approximately one percent of that in the current study area. The authors reported that SOC contents decreased in the topsoil but increased in the subsoil within 100 a.

5. Conclusions

To better represent the turnover of SOC, lateral C migration was simulated in terms of neighbourhood variables in the HCA model. In this study, we assumed that land use and climate change mainly affected the SOC dynamics. HCA enhanced the prediction performance by 15.27% over MLR, 12.31% over SVM and 10.98% over KED. The simulation results revealed that the SOC concentration in this area would continuously increase with increases in both the MAAT and MAP. This area has undergone long-term urbanization, in which the mean SOC values of villages are slightly higher than those of cropland due to the large amounts of green manure in urban-rural ecotones and high C sequestration in urban parks. The SOC concentration increased with the rapid growth of urbanization, during which more organic matter is supplied and a larger area might be occupied by green spaces. Regarding the complex process of soil evolution, our proposal provides a viable alternative for SOC dynamics simulation.

Acknowledgements

Funding for this study was provided by the National Key Research and Development Program of China (No. 2017YFA0603002) and the National Natural Science Foundation of China (grant No. 41571130051, No. 41771251, No. 41571212 and No. 41501228).

Appendix A. Supplementary data

Supplementary material related to this article can be found, in the online version, at doi:https://doi.org/10.1016/j.agee.2018.09.034.

References

Aburas, M.M., Ho, Y.M., Ramli, M.F., Ash'aari, Z.H., 2016. The simulation and prediction of spatio-temporal urban growth trends using cellular automata models: a review. Int. J. Appl. Earth Observ. Geoinf. 52, 380–389.
Almagro, M., Martínez-Mena, M., 2014. Litter decomposition rates of green manure as affected by soil erosion, transport and deposition processes, and the implications for the soil carbon balance of a rainfed olive grove under a dry Mediterranean climate. Agric. Ecosyst. Environ. 196, 167–177.
Bae, J., Ryu, Y., 2015. Land use and land cover changes explain spatial and temporal variations of the soil organic carbon stocks in a constructed urban park. Landsc. Urban Plan. 136, 57–67.
Barthold, F.K., Wiesmeier, M., Breuer, L., Frede, H.G., Wu, J., Blank, F.B., 2013. Land use and climate control the spatial distribution of soil types in the grasslands of Inner Mongolia. J. Arid Environ. 88 (1), 194–205.
Basse, R.M., Omrani, H., Charif, O., Gerber, P., Bódis, K., 2014. Land use changes modelling using advanced methods: cellular automata and artificial neural networks. The spatial and explicit representation of land cover dynamics at the cross-border region scale. Appl. Geogr. 53, 160–171.
Bishop, T.F.A., McBratney, A.B., Laslett, G.M., 1999. Modelling soil attribute depth functions with equal–area quadratic smoothing splines. Geoderma 91, 27–45.
Bodaghabadi, M.B., Salehi, M.H., Martínez-Casasnovas, J.A., Mohammadi, J., Toomanian, N., Borujeni, I.E., 2011. Using Canonical Correspondence Analysis (CCA) to identify the most important DEM attributes for digital soil mapping applications. Catena 86 (1), 66–74.
Brilli, L., Bechini, L., Bindi, M., Carozzi, M., Cavalli, D., Conant, R., Dorich, C.D., Doro, L., Ehrhardt, F., Farina, R., Ferrise, R., Fitton, N., Francaviglia, R., Grace, P., Iocola, I., Klumpp, K., Léonard, J., Martin, R., Massad, R.S., Recous, S., Seddaiu, G., Sharp, J., Smith, P., Smith, W.N., Soussana, J.F., Bellocchi, G., 2017. Review and analysis of strengths and weaknesses of agro-ecosystem models for simulating C and N fluxes. Sci. Total Environ. 598, 445–470.
Brus, D.J., Kempen, B., Heuvelink, G.B.M., 2011. Sampling for validation of digital soil maps. Eur. J. Soil Sci. 62 (3), 394–407.
Chuai, X.W., Huang, X.J., Wang, W.J., Zhang, M., Lai, L., Liao, Q.L., 2012. Spatial variability of soil organic carbon and related factors in Jiangsu Province. Pedosphere 22 (3), 404–414.
Cooperative Research Group on Chinese Soil Taxonomy, 2001. Chinese Soil Taxonomy. Science Press, Beijing.
de Gruijter, J.J., Brus, D.J., Bierkens, M.F.P., Knotters, M., 2006. Sampling for Natural Resource Monitoring. Springer, Berlin.
Dorendorf, J., Eschenbach, A., Schmidt, K., Jensen, K., 2015. Both tree and soil carbon need to be quantified for carbon assessments of cities. Urban For. Urban Green. 14, 447–455.
Dorji, T., Odeh, I.O.A., Field, D.J., Baillie, I.C., 2014. Digital soil mapping of soil organic carbon stocks under different land use and land cover types in montane ecosystems, Eastern Himalayas. For. Ecol. Manage. 318 (3), 91–102.
ESRI, 2014. ArcGIS Desktop: Release 10.2. Environmental Systems Research Institute, Redlands, CA.
Fonstad, M.A., 2013. Cellular automata in geomorphology. Treatise on Geomorphology 2, 117–134.
Gao, J., Liang, C., Shen, G., Lv, J., Wu, H., 2017. Spectral characteristics of dissolved organic matter in various agricultural soils throughout China. Chemosphere 176, 108–116.
Garcia-Franco, N., Albaladejo, J., Almagro, M., Martínez-Mena, M., 2015. Beneficial effects of reduced tillage and green manure on soil aggregation and stabilization of organic carbon in a Mediterranean agroecosystems. Soil Tillage Res. 153, 66–75.
Gelaw, A.M., Singh, B.R., Lal, R., 2014. Soil organic carbon and total nitrogen stocks under different land uses in a semi-arid watershed in Tigray, Northern Ethiopia. Agric. Ecosyst. Environ. 188, 256–263.

Grunwald, S., 2009. Multi–criteria characterization of recent digital soil mapping and modeling approaches. Geoderma 152 (3–4), 195–207.
Guo, P.T., Li, M.F., Luo, W., Tang, Q.F., Liu, Z.W., Lin, Z.M., 2015. Digital mapping of soil organic matter for rubber plantation at regional scale: an application of random forest plus residuals kriging approach. Geoderma 237–238, 49–59.
Harris, P., Brunsdon, C., Fotheringham, A.S., 2011. Links, comparisons and extensions of the geographically weighted regression model when used as a spatial predictor. Stoch. Environ. Res. Risk Assess. 25, 123–138.
He, Y.T., He, X.H., Xu, M.G., Zhang, W.J., Yang, X.Y., Huang, S.M., 2018. Long-term fertilization increases soil organic carbon and alters its chemical composition in three wheat-maize cropping sites across central and south China. Soil Tillage Res. 177, 79–87.
Heung, B., Ho, H.C., Zhang, J., Knudby, A., Bulmer, C.E., Schmidt, M.G., 2016. An overview and comparison of machine-learning techniques for classification purposes in digital soil mapping. Geoderma 265, 62–77.
Hijmans, R.J., Cameron, S.E., Parra, J.L., Jones, P.G., Jarvis, A., 2005. Very high resolution interpolated climate surfaces for global land areas. Int. J. Climatol. 25, 1965–1978.
Hutyra, L., Yoon, B., Alberti, M., 2011. Terrestrial carbon stocks across a gradient of urbanization: a study of the Seattle, WA region. Glob. Chang. Biol. 17 (2), 783–797.
Jandl, R., Rodeghiero, M., Martinez, C., Cotrufo, M.F., Bampa, F., Wesemael, B.V., Harrison, R.B., Guerrini, I.A., Richter, Jr.D.D., Rustad, L., Lorenz, K., Chabbi, A., Miglietta, F., 2014. Current status, uncertainty and future needs in soil organic carbon monitoring. Sci. Total Environ. 468–469, 376–383.
Jiang, G.Y., Xu, M.G., He, X.H., Zhang, W.J., Huang, S.M., Yang, X.Y., Liu, H., Peng, C., Shirato, Y., Iizumi, T., Wang, J.Z., Murphy, D.V., 2014. Soil organic carbon sequestration in upland soils of northern China under variable fertilizer management and climate change scenarios. Glob. Biogeochem. Cycles 28 (3), 319–333.
Jiménez, A., 2013. Cellular automata to describe seismicity: a review. Acta Geophys. 61 (6), 1325–1350.
Kempen, B., Brus, D.J., Stoorvogel, J.J., 2011. Three-dimensional mapping of soil organic matter content using soil type-specific depth functions. Geoderma 162 (1–2), 107–123.
Leifeld, J., Bassin, S., Fuhrer, J., 2005. Carbon stocks in Swiss agricultural soils predicted by land-use, soil characteristics, and altitude. Agric. Ecosyst. Environ. 105, 255–266.
Li, D., Shao, M., 2014. Soil organic carbon and influencing factors in different landscapes in an arid region of northwestern China. Catena 116, 95–104.
Li, X., Yeh, A.G.O., 2002. Neural-network-based cellular automata for simulating multiple land use changes using GIS. Int. J. Geogr. Inf. Sci. 16 (4), 323–343.
Li, S., Li, J., Li, C., Huang, S., Li, X., Li, S., Ma, Y., et al., 2016a. Testing the RothC and DNDC models against long-term dynamics of soil organic carbon stock observed at cropping field soils in North China. Soil Tillage Res. 163, 290–297.
Li, B., Chen, D., Wu, S., Zhou, S., Wang, T., Chen, H., 2016b. Spatio-temporal assessment of urbanization impacts on ecosystem services: Case study of Nanjing City, China. Ecol. Indic. 71, 416–427.
Ließ, M., Glaser, B., Huwe, B., 2012. Making use of the World Reference Base diagnostic horizons for the systematic description of the soil continuum—application to the tropical mountain soil-landscape of southern Ecuador. Catena 97, 20–30.
López-Ulloa, M., Veldkamp, E., de Koning, G.H.J., 2005. Soil carbon stabilization in converted tropical pastures and forests depends on soil type. Soil Sci. Soc. Am. J. 69, 1110–1117.
Mendicino, G., Pedace, J., Senatore, A., 2015. Stability of an overland flow scheme in the framework of a fully coupled eco-hydrological model based on the Macroscopic Cellular Automata approach. Commun. Nonlinear Sci. Numer. Simul. 21 (1–3), 128–146.
Meyer, D., Dimitriadou, E., Hornik, K., Weingessel, A., Leisch, F., Chang, C.C., Lin, C.C., 2017. e1071: Misc Functions of the Department of Statistics, Probability Theory Group (Formerly: E1071), TU Wien. R Package Version 1.6–8. Available at:. https://CRAN.R-project.org/package=e1071.
Muñoz-Rojas, M., Abd-Elmabod, S.K., Zavala, L.M., Rosa, D.D.L., Jordán, A., 2017. Climate change impacts on soil organic carbon stocks of Mediterranean agricultural areas: a case study in Northern Egypt. Agric. Ecosyst. Environ. 238, 142–152.
Nelson, D.W., Sommers, L.E., 1982. Total carbon, organic carbon and organic matter. In: In: Page, A.L., Miller, R.H., Keeney, D. (Eds.), Methods of Soil Analysis, Part 2. Chemical and Microbiological Properties. Agronomy Monograph 9. ASA and SSSA, Madison, WI, pp. 539–579.
Oku, M., Aihara, K., 2010. Noise-robust realization of Turing-complete cellular automata by using neural networks with pattern representation. Phys. Lett. A 374 (48), 4859–4863.
Ouyang, W., Shan, Y., Hao, F., Lin, C., 2014. Differences in soil organic carbon dynamics in paddy fields and drylands in northeast China using the CENTURY. Agric. Ecosyst. Environ. 194, 38–47.
Parton, W.J., Schimel, D.S., Cole, C.V., Ojima, D.S., 1987. Analysis of factors controlling soil organic matter levels in Great Plains Grasslands. Soil Sci. Soc. Am. J. 51 (5), 1173–1179.
Paz, C.P., Goosem, M., Bird, M., Preece, N., Goosem, S., Fensham, R., Laurance, S., 2016. Soil types influence predictions of soil carbon stock recovery in tropical secondary forests. For. Ecol. Manage. 376, 74–83.
Pebesma, E.J., 2004. Multivariable geostatistics in S: the gstat package. Comput. Geosci. 30 (7), 683–691.
Raciti, S.M., Hutyra, L.R., Finzi, A.C., 2012. Depleted soil carbon and nitrogen pools beneath impervious surfaces. Environ. Pollut. 164, 248–251.
Ravazzani, G., Rametta, D., Mancini, M., 2011. Macroscopic cellular automata for groundwater modelling: a first approach. Environ. Model. Softw. 26 (5), 634–643.
Ross, C.W., Grunwald, S., Myers, D.B., Xiong, X., 2016. Land use, land use change and soil carbon sequestration in the St. Johns River Basin, Florida, USA. Geoderma Reg. 7 (1), 19–28.
Sallustio, L., Quatrini, V., Geneletti, D., Corona, P., Marchetti, M., 2015. Assessing land take by urban development and its impact on carbon storage: findings from two case studies in Italy. Environ. Impact Assess. Rev. 54, 80–90.
Shen, C., Yan, Y., 2017. A new tool for spatiotemporal pattern decomposition based on empirical mode decomposition: a case study of monthly mean precipitation in Taihu Lake Basin, China. J. Atmos. Solar–Terrestrial Phys. 154, 10–20.
Song, X., Zhang, G., Liu, F., Li, D., Zhao, Y., Yang, J., 2016. Modeling spatio-temporal distribution of soil moisture by deep learning-based cellular automata model. J. Arid Land 8 (5), 734–748.
Stocchero, A., Seadon, J.K., Falshaw, R., Edwards, M., 2017. Urban equilibrium for sustainable cities and the contribution of timber buildings to balance urban carbon emissions: a New Zealand case study. J. Clean. Prod. 143, 1001–1010.
Taghizadeh-Mehrjardi, R., Nabiollahi, K., Kerry, R., 2016. Digital mapping of soil organic carbon at multiple depths using different data mining techniques in Baneh region, Iran. Geoderma 266, 98–110.
The National Soil Survey Office, 1995. Soil Species of China Vol. 1 China Agriculture Press, Beijing (in Chinese).
Vasenev, V.I., Stoorvogel, J.J., Vasenev, I.I., Valentini, R., 2012. How to map soil organic carbon stocks in highly urbanized regions? Geoderma 226–227, 103–115.
Wang, Y., Li, S., 2011. Simulating multiple class urban land-use/cover changes by RBFN-based CA model. Comput. Geosci. 37 (2), 111–121.
Wang, Y., Fang, N., Zhang, F., Wang, L., Wu, G., Yang, M., 2017. Effects of erosion on the microaggregate organic carbon dynamics in a small catchment of the Loess Plateau, China. Soil Tillage Res. 174, 205–213.
Wei, S., Zhang, X., Mclaughlin, N.B., Chen, X., Jia, S., Liang, A., 2017. Impact of soil water erosion processes on catchment export of soil aggregates and associated SOC. Geoderma 294, 63–69.
Were, K., Bui, D.T., Dick, Ø.B., Singh, B.R., 2015. A comparative assessment of support vector regression, artificial neural networks, and random forests for predicting and mapping soil organic carbon stocks across an Afromontane landscape. Ecol. Indic. 52, 394–403.
Wilkinson, G.N., Rogers, C.E., 1973. Symbolic descriptions of factorial models for analysis of variance. Appl. Stat. 22, 392–399.
Xiong, X., Grunwald, S., Myers, D.B., Ross, C.W., Harris, W.G., Comerford, N.B., 2014. Interaction effects of climate and land use/land cover change on soil organic carbon sequestration. Sci. Total Environ. 493, 974–982.
Ye, H.C., Huang, Y.F., Chen, P.F., Huang, W.J., Zhang, S.W., Huang, S.Y., Hou, S., 2016. Effects of land use change on the spatiotemporal variability of soil organic carbon in an urban-rural ecotone of Beijing, China. J. Integr. Agric. 15 (4), 918–928.
Yigini, Y., Panagos, P., 2016. Assessment of soil organic carbon stocks under future climate and land cover changes in Europe. Sci. Total Environ. 557–558, 838–850.
Yong, L., Cheng, W., Yue, W., Hu, Y., 2013. Storage and density of soil organic carbon in urban topsoil of hilly cities: a case study of Chongqing Municipality of China. Chin. Geogr. Sci. 23 (1), 26–34.
Yoon, T.K., Seo, K.W., Park, G.S., Son, Y.M., Son, Y., 2016. Surface soil carbon storage in urban green spaces in three major South Korean cities. Forests 7 (6), 115.
Yu, Y., Huang, Y., Zhang, W., 2012. Modeling soil organic carbon change in croplands of China, 1980–2009. Glob. Planet. Change 82–83, 115–128.
Yu, Y., Huang, Y., Zhang, W., 2013. Projected changes in soil organic carbon stocks of China's croplands under different agricultural managements, 2011–2050. Agric. Ecosyst. Environ. 178, 109–120.
Zhang, W., Huang, B., Luo, D., 2014. Effects of land use and transportation on carbon sources and carbon sinks: a case study in Shenzhen, China. Landsc. Urban Plan. 122 (2), 175–185.
Zhang, L., Zhuang, Q., He, Y., Liu, Y., Yu, D., Zhao, Q., 2016a. Toward optimal soil organic carbon sequestration with effects of agricultural management practices and climate change in Tai-Lake paddy soils of China. Geoderma 275, 28–39.
Zhang, X., Xu, M., Sun, N., Xiong, W., Huang, S., Wu, L., 2016b. Modelling and predicting crop yield, soil carbon and nitrogen stocks under climate change scenarios with fertiliser management in the North China Plain. Geoderma 265, 176–186.
Zhao, M.S., Zhang, G.L., Wu, Y.J., Li, D.C., Zhao, Y.G., 2015. Driving forces of soil organic matter change in Jiangsu Province of China. Soil Use Manag. 31 (4), 440–449.